Stripe quadrupole order in the nematic phase of $FeSe_{1-x}S_x$

W.-L. Zhang,[1,*] S.-F. Wu,[1,†] S. Kasahara,[2] T. Shibauchi,[3] Y. Matsuda,[2] and G. Blumberg[1,4,‡]

[1] *Department of Physics & Astronomy, Rutgers University, Piscataway, New Jersey 08854, USA*
[2] *Department of Physics, Kyoto University, Kyoto, 606-8502, Japan*
[3] *Department of Advanced Materials Science, University of Tokyo, Kashiwa, Chiba 277-8561, Japan*
[4] *National Institute of Chemical Physics and Biophysics, Akadeemia tee 23, 12618 Tallinn, Estonia*

(Dated: January 23, 2018)

We use polarization-resolved electronic Raman spectroscopy to study charge dynamics in non-magnetic $FeSe_{1-x}S_x$ superconductor. We observe two features of the XY quadrupole symmetry: a low-energy quasi-elastic peak (QEP) and an electronic continuum. The QEP exhibits critical enhancement upon cooling towards the structural transition at $T_S(x)$. Below $T_S(x)$, the QEP diminishes gradually, and a gap with temperature evolution reminiscent of a mean-field order parameter opens up in the continuum. The intensity of the QEP develops with increasing sulfur doping x and maximizes at $x \approx 0.15$, while the gap magnitude decreases with the suppression of $T_S(x)$. We interpret the development of the gap in the quadrupole scattering channel as the formation of a stripe quadrupole order: a wave of quadrupole moment without charge or spin modulation.

The iron-based superconductors (FeSCs) exhibit a complex phase diagram with multiple competing orders. For most of the FeSCs, an electronic nematic phase transition takes place at T_S, which is closely followed by a magnetic phase transition at T_N [1–4]. Superconductivity emerges in close proximity to the electronic nematic and the antiferromagnetic orders. The highest superconducting (SC) transition temperature T_C often occurs when the nematic and the magnetic orders are fully suppressed but the orbital/charge or spin fluctuations remain strong [5–8]. The relationship between these fluctuations and superconductivity has been a focus of intense research [4, 9–15].

FeSe crystals provide the simplest case to elucidate the relationship between the orbital/charge order and superconductivity because it shows nematicity in the absence of magnetic order [9, 18, 19]. At ambient pressure, a structural phase transition that breaks the four-fold rotational symmetry (C_4) takes place at $T_S = 90$ K. Strong electronic quadrupole fluctuations involving the charge transfer between the Fe $3d_{xz}$ and $3d_{yz}$ orbitals, which contribute to most of the electronic density of states near E_F, have been observed above T_S [20–23]. The degeneracy of the d_{xz} and d_{yz} orbitals is lifted in the broken symmetry phase [24–26]. In the orthorhombic phase, although the lattice is only weakly distorted, prominent anisotropy is found for many electronic properties [16, 27]. For crystals, superconductivity emerges in the nematic phase at $T_C \approx 9$ K [18], while for FeSe monolayer films deposited on $SrTiO_3$ substrate, T_C can be enhanced above 100 K [28–30]. Orbital-selective SC pairing has been reported by ARPES and quasiparticle interference (QPI) in bulk FeSe: the SC gap energy is large only for specific region of the nematic Fermi surfaces with the d_{yz} orbital characters [16, 27, 31]. However, the mechanism behind the puzzling orbital-selective superconductivity has not been discussed in depth.

In this Letter, we employ polarization-resolved Raman spectroscopy to study charge quadrupole dynamics in non-magnetic superconductor $FeSe_{1-x}S_x$ [20, 32]. We observe two main features in the XY symmetry scattering channel: a low-energy quasi-elastic peak (QEP) and a high-energy electronic continuum. Above $T_S(x)$, the QEP exhibits critical enhancement and softening upon cooling in wide temperature and doping range. Below $T_S(x)$, an unexpected gap gradually develops in the spectra of the electronic continuum. Temperature dependence of the gap scales with the orthorhombic order parameter. The gap magnitude is proportional to $T_S(x)$

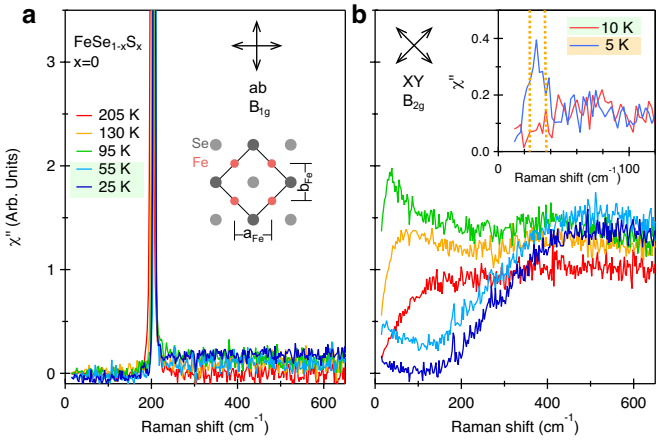

FIG. 1. Temperature evolution of the $B_{1g}(ab)$ and $B_{2g}(XY)$ symmetry Raman response $\chi''(\omega, T)$ for pristine FeSe. Inset of (a) shows the top view of the FeSe layer. Dark and light gray circles represent the Se above and below the Fe layer. The 2-Fe unit cell for the high-temperature phase is shown by solid lines. In the low-temperature phase, the nearest Fe-Fe bonding distance a_{Fe} becomes larger than b_{Fe} while a_{Fe} and b_{Fe} remain orthogonal. Inset of (b): $\chi''(\omega, T)$ in the XY symmetry channel of FeSe in the normal state (10 K) and SC state (5 K). The magnitude of the two superconducting gaps $2\Delta_{SC} = 3$ and 4.6 meV measured by tunneling spectroscopy are shown with the vertical dotted lines [16, 17].

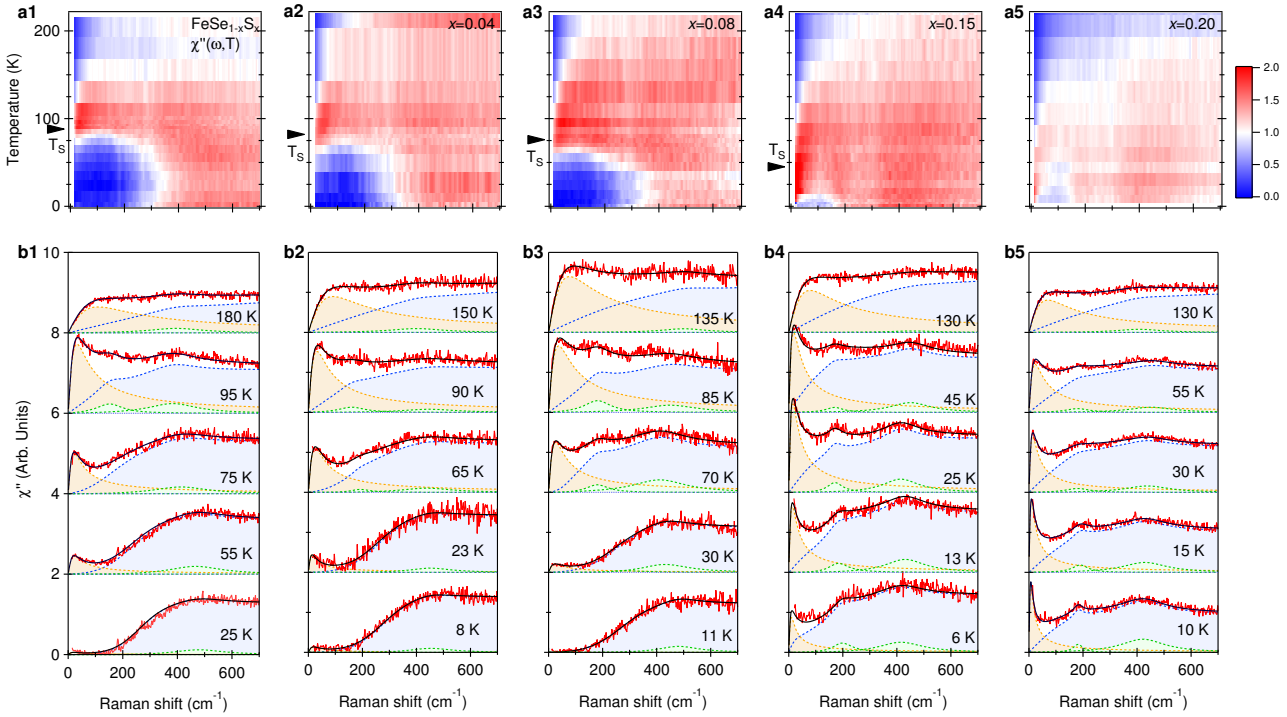

FIG. 2. (a1-a5) Temperature evolution of the XY symmetry Raman susceptibility $\chi''(\omega, T)$ for $FeSe_{1-x}S_x$ (x = 0, 0.04, 0.08, 0.15 and 0.2). Arrows at the temperature axis denote $T_S(x)$. (b1-b5) $\chi''(\omega, T)$ (red) at representative temperatures and their fits (black) with the decompositions of the QEP χ''_{QEP} (orange shade) and the continuum $\chi''_C \times \Theta$ (blue shade). The two Lorentz oscillators χ''_L at around 190 and 450 cm^{-1} are shown in green shade.

with the ratio $2\Delta_x(0)/k_B T_S(x) = 4.8$. We interpret the development of the gap in the quadrupole scattering channel as the formation of a stripe quadrupole (SQ) order below $T_S(x)$, which could provide explanations for the observed orbital-selective superconductivity.

$FeSe_{1-x}S_x$ (x = 0, 0.04, 0.08, 0.15 and 0.2) single crystals were grown by chemical vapor transport technique as described in [20]. By substitution of sulfur for selenium, T_S is suppressed but the system remains non-magnetic, and superconductivity remains robust [20, 31, 32]. Strain-free crystals were cleaved in nitrogen atmosphere and positioned in a continuous flow optical cryostat. Polarization-resolved Raman spectra were acquired in a quasi-backscattering geometry from the ab surface. We used 2.6 eV excitation from a Kr^+ laser. The laser power was kept below 10 mW for most measurements and less than 2 mW for the measurements in the superconducting state. The laser heating temperature $\approx$ 1 K/mW was calibrated by the appearance of the stripe pattern on the crystal surface at T_S [33]. The Raman scattering signal was analyzed by a custom triple-grating spectrometer and the data were corrected for the spectral response of the spectrometer.

Figs. 1 show the temperature dependence of the Raman response for the pristine FeSe B_{1g} (ab) and B_{2g} (XY) symmetry channels of the D_{4h} group defined in the 2-Fe unit cell. B_{1g} channel contains the Fe phonon ($\approx$ 195 cm^{-1}) [34] on a weak continuum background (Fig. 1a). In contrast, the electronic Raman continuum in the B_{2g} channel (Fig. 1b) is strong and is composed of two main features with a remarkable temperature dependence:

(1) *A low-energy quasi-elastic scattering peak (QEP).* The intensity of the QEP is weak at high temperatures. Upon cooling, it softens, gains intensity, reaches its maximum intensity just above $T_S(x)$, and then gradually loses its intensity below $T_S(x)$ (Fig. 2b1). In the supercon-

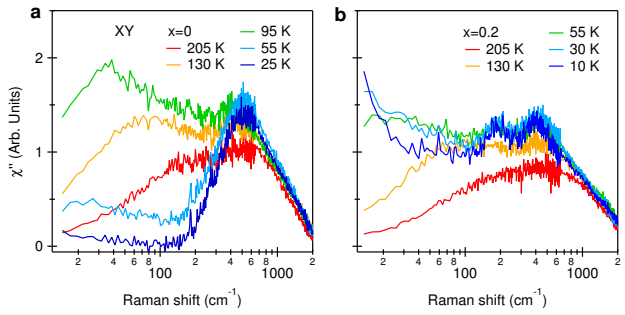

FIG. 3. Temperature evolution of the XY symmetry Raman response $\chi''(\omega, T)$ for (a) FeSe and (b) $FeSe_{0.8}S_{0.2}$.

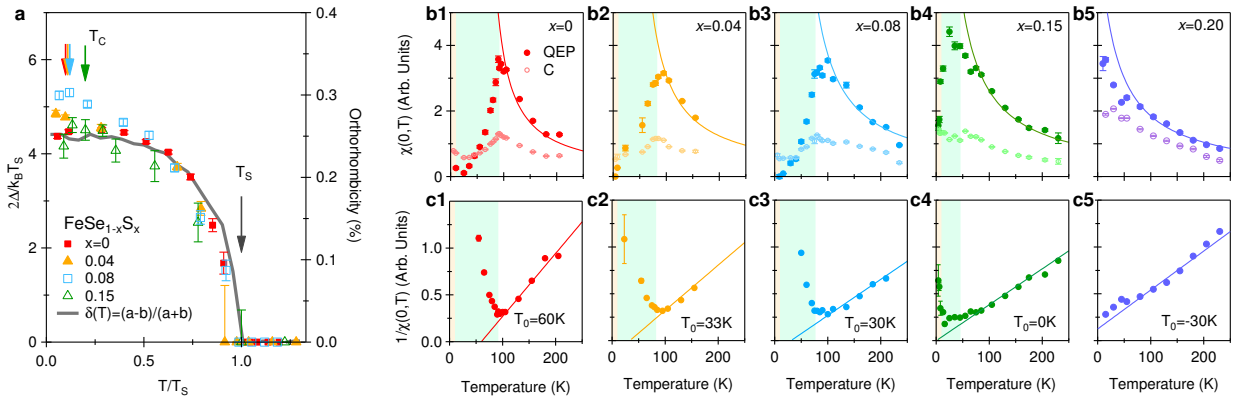

FIG. 4. (a) Temperature and doping evolution of the nematic gap $2\Delta(T)/k_BT_S$ in $FeSe_{1-x}S_x$ as a function of the reduced temperature T/T_S. The gray curve is the lattice order parameter $\delta(T)$ = (a-b)/(a+b) for FeSe from ref [35]. T_S and T_C are denoted by arrows. (b1-b5) Static Raman susceptibility $\chi_{QEP}(0,T)$ and $\chi_C(0,T)$ for x = 0, 0.04, 0.08, 0.15 and 0.2. Curie-Weiss fit for χ_{QEP}(0,T) at $T > T_S$ is shown by the solid curve. The yellow and cyan shades indicate $T_C(x)$ and $T_S(x)$, respectively. (c1-c5) Temperature dependence of the inverse static susceptibility $1/\chi_{QEP}$(0,T) and the Weiss temperature $T_0(x)$. Error bars are the fitting standard errors.

ducting phase, the QEP acquires coherence and undergoes a metamorphosis into a coherent in-gap collective mode [36–40] (inset Fig. 1b).

(2) *A broad electronic continuum.* The intensity of the continuum for 400-2000 cm^{-1} (Fig. 3a) shows weak and monotonic increase with cooling above $T_S(x)$. A broad peak centered near 450 cm^{-1} gradually appears below 100 K. An additional weak feature at around 190 cm^{-1} appears at temperatures close to T_S. Below $T_S(x)$, a significant gap suppression develops below 400 cm^{-1}.

For doped crystals, temperature evolution of the XY Raman response is quite similar to pristine FeSe (Figs. 2a1-a5). The 450 cm^{-1} peak appears at low temperature for all sulfur contents in both the tetragonal and orthorhombic phase (Figs. 3a-b). Hence, the feature is not exclusive for the nematic phase. The intensity of the 190 cm^{-1} peak increases with S doping; for $x \leq 0.08$ samples, the feature is suppressed at low temperatures when gap with higher than the feature energy opens.

In the orthorhombic phase, at the lowest temperature, a full gap suppression is observed for all doping concentrations except for $x = 0.15$, where a reduced scattering intensity remains in the gap. For $x = 0.2$, which remains tetragonal structure in whole temperature range, no gap suppression is observed.

We perform a multi-component fit to the XY symmetry Raman response (Figs. 2b1-b5). Here we represent QEP as a Drude function $\chi''_{QEP}(\omega,T) = A^2_{QEP}\omega\Gamma_{QEP}/(\omega^2+\Gamma^2_{QEP})$, and the electronic continuum as $\chi''_C(\omega,T) = A^2_C \tanh[\omega/\Gamma_C] + \chi''_L(\omega,T)$, where $\chi''_L(\omega,T)$ is for the Lorentz oscillators centered around 190 and 450 cm^{-1}. For $x \leq 0.15$, below $T_S(x)$, the gap-like suppression is modeled by $\Theta(\omega,T) = \frac{1}{2}(1+\tanh[\frac{\omega-2\Delta(T)}{2k_BT_{eff}}])$ and applied to the continuum, where $2\Delta(T)$ is the gap energy and T_{eff} is an effective temperature. $\Gamma_C(T)$ follows a quadratic temperature dependence for all samples except for sulfur composition in the vicinity of the critical doping $x \approx 0.17$ [20], where the temperature dependence is nearly linear [17].

The reduced gap energy $2\Delta_x(T)/k_BT_S(x)$ collapses to a universal temperature dependence with $2\Delta_x(0)/k_BT_S(x) = 4.8$ (Fig. 4a). The temperature dependence of $2\Delta_x(T)$ follows the lattice order parameter $\delta(T) = (a+b)/(a-b)$[35], manifesting the direct connection between the formation of the gap and the lattice orthorhombicity.

We calculate the static Raman susceptibility for the QEP and the continuum contributions, $\chi_{QEP}(0,T)$ and $\chi_C(0,T)$, by Kramers-Kronig transformation [17]. In contrast to the mild temperature evolution of $\chi_C(0,T)$, a critical enhancement is seen above $T_S(x)$ for $\chi_{QEP}(0,T)$ (Figs. 4b1-b5). The temperature dependence of the QEP is generic for most FeSCs [5, 22, 33, 38, 41], and has been related to the ferro-quadrupole (FQ) fluctuations of a d-wave Pomeranchuk instability at q=0 [12, 38, 41–46]. The charge transfer between the nearly degenerate d_{xz} and d_{yz} orbitals creates charge quadrupole with moment proportional to the local charge imbalance $Q \propto n_{d_{xz}} - n_{d_{yz}}$. In Fig. 5b we illustrate a snapshot of the FQ fluctuations. Such excitation results in a $\Gamma^+_4(B_{2g})$ symmetry dynamic deformation of the Fermi surface pockets with nodal lines in the X/Y directions. We fit $\chi_{QEP}(0, T > T_S)$ with a Curie-Weiss function $\chi_{QEP}(0,T) \propto Q^2(x)/(T - T_0(x))$ (Fig. 4c1-c5), where $T_0(x)$ is the Weiss temperature [5, 38].

In Fig. 5a we display the fitting parameters $Q(x)$, $2\Delta_x(0)$ and $T_0(x)$ together with the $FeSe_{1-x}S_x$ phase diagram. $T_0(x)$ is tens of K below T_S, decreases with

x and vanishes at $x \approx 0.15$, close to the nematic quantum critical point (QCP) as it was reported by elastoresistence study [20]. $Q(x)$ increases with x and maximizes at $x \approx 0.15$, while $2\Delta_x(0)$ decreases with x, implying that the QEP and the gapped continuum arise from competing instabilities.

Now we turn to the origin of the gap. Such gap cannot be described by non-interacting electron-hole excitations between the d_{xz}/d_{yz} orbitals: the gap energy in Raman spectra is inconsistent with the energy of any d_{xz}/d_{yz} bare electron-hole excitation in FeSe [24–26, 47]. Appearance of the gap only in the XY symmetry channel reveals a hidden density wave in either a_{Fe} or b_{Fe} direction [48]. Because neither charge nor spin modulation in the nematic phase was detected [18], the possibilities of charge/spin density wave gap are ruled out. We propose a collinear stripe d_{zx}/d_{yz} quadrupole order consisting of staggered Q and $-Q$ quadrupole moments, as shown in Fig. 5c. The order parameter in real space can be defined as $\phi_{XY} = \prod_{r=A\,site} |Q_r\rangle \times \prod_{r=B\,site} |\bar{Q}_r\rangle$, which would give rise to the XY symmetry gap. Here $Q/-Q$ quadrupole moments reside on iron sites r = A/B.

Both, ARPES data and RG calculations show that the orbital order parameter involving the d_{xz} and d_{yz} orbitals at M_X/M_Y points have nearly equivalent magnitude but opposite sign [24–26, 47]. Such nearly equal total occupation of these two orbitals can be realized by the SQ, rather than the FQ order.

XY symmetry Raman scattering directly couples to $\Delta L = 2$ quadrupole excitations, making it a unique tool to probe the SQ order parameter or its dynamical fluctuations. In contrast, given that the total charge on each Fe site $n_r = n_{r,d_{xz}} + n_{r,d_{yz}}$ is preserved, the charge sensitive probes such as scanning tunneling spectroscopy, X-ray diffraction or optical conductivity are unresponsive to such SQ order. We also notice that neutron scattering works suggest a hidden collinear antiferromagnetic quadrupole (AFQ) order for in FeSe [49, 50]. If the magnetic AFQ is at the same ordering vector as the charge SQ, a bilinear coupling between these two orders is allowed.

In the SQ-ordered phase, if the charge of the d_{xz} orbitals is modulated along the a-direction but remains invariant along the b-direction for the d_{yz} orbitals (Fig. 5c), the quasi-particle weight Z_{xz} in the d_{xz} orbitals would be suppressed. The reduction of Z_{xz} would naturally result in a smaller SC gap for the d_{xz} orbitals [51] and overall in suppression of T_C, consistent with the observation of *orbital-dependent superconducting gap* reported by ARPES and QPI [16, 27]. On the other hand, due to the coupling to the substrate, the SQ fluctuations are expected to be removed for the high-T_C monolayer FeSe films deposited on the $SrTiO_3$, resulting in a high-T_C phenomenon [28, 29, 52].

In summary, we use polarization-resolved Raman spectroscopy to study the evolution of charge dynamics in

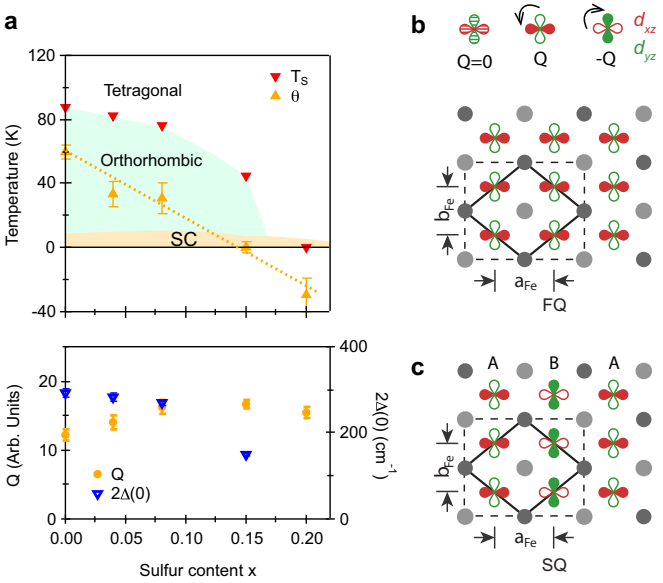

FIG. 5. (a) Phase diagram and the fitting parameters in $FeSe_{1-x}S_x$. The FQ moment $Q(x)$ (empty squares, lower panel) and the Weiss temperature $T_0(x)$ (upward triangles, upper panel) are obtained from the Curie-Weiss fit of $\chi_{QEP}(0,T)$. $\Delta_x(0)$ (downward triangles, lower panel) is obtained from $\Delta_x(T)$. (b) A snapshot of the B_{2g} symmetry FQ fluctuations consist of d_{xz}/d_{yz} charge quadrupoles from the top view of a FeSe layer. An elementary quadrupole Q moment is created by on-site charge transfer from d_{yz} to d_{xz} orbital while a quadrupole moment $-Q$ is created by charge transfer from d_{xz} to d_{yz} orbital. (c) SQ ground state with staggered $|Q\rangle$ ($A\,site$) and $|\bar{Q}\rangle$ ($B\,site$) in vertical stripes. $a_{Fe} > b_{Fe}$.

nonmagnetic $FeSe_{1-x}S_x$ superconductor as a function of sulfur doping and temperature at above and below $T_S(x)$. We observe the development of a QEP on cooling towards $T_S(x)$ and a pronounced gap in the XY symmetry continuum below $T_S(x)$. By increasing sulfur concentration, the QEP intensity is enhanced, while the gap magnitude and $T_S(x)$ decrease. The ferro-quadrupole fluctuations are strongest in the vicinity of the nematic critical point at $x_{cr} \approx 0.15$. The appearance of robust low-energy gap implies the formation of a long-range quadrupole order, for example, a staggered stripe order. In the presence of the SQ order, the superconductivity on the d_{xz} orbital is suppressed due to the reduction of the quasi-particle weight along the SQ ordering vector direction, which provides a natural explanation for the observed orbital-selective superconductivity in bulk FeSe [16, 27] as well as for the phenomena of high-T_C superconductivity in monolayer FeSe films [28, 29] where the SQ order is expected to be suppressed due to the coupling to the substrate.

We thank A. V. Chubukov, T. P. Devereaux, T. Dong, K. Haule, H.-H. Kung, M. Khodas, P. Richard, J. Schmalian and Q.-M. Si for valuable discussions. The

work at Rutgers was supported by the U.S. Department of Energy, Office of Basic Energy Sciences, Division of Materials Sciences and Engineering under Contract No. DE-SC0005463. The work in Japan was supported by Grant-in-Aids for Scientific Research (Proposals No. 15H02106, 15H03688, and 25220710), and by Grant-in-Aids on Innovative Areas "Topological Materials Science" (No. 15H05852), from Japan Society for the Promotion of Science (JSPS). GB acknowledges the hospitality of the Aspen Center for Physics, which is supported by NSF grant PHY-1607611.

* wz131@physics.rutgers.edu
† On leave from Beijing National Laboratory for Condensed Matter Physics and Institute of Physics, Chinese Academy of Sciences, Beijing, 100190, China
‡ girsh@physics.rutgers.edu

[1] E. Fradkin, S. A. Kivelson, M. J. Lawler, J. P. Eisenstein, and A. P. Mackenzie, Annu. Rev. Condens. Matter Phys. **1**, 153 (2010).
[2] G. R. Stewart, Rev. Mod. Phys. **83**, 1589 (2011).
[3] J. Paglione and R. L. Greene, Nat Phys **6**, 645 (2010).
[4] R. M. Fernandes, A. V. Chubukov, and J. Schmalian, Nat. Phys. **10**, 97 (2014).
[5] Y. Gallais, R. M. Fernandes, I. Paul, L. Chauvière, Y.-X. Yang, M.-A. Méasson, M. Cazayous, A. Sacuto, D. Colson, and A. Forget, Phys. Rev. Lett. **111**, 267001 (2013).
[6] A. E. Bohmer, P. Burger, F. Hardy, T. Wolf, P. Schweiss, R. Fromknecht, M. Reinecker, W. Schranz, and C. Meingast, Phys. Rev. Lett. **112**, 047001 (2014).
[7] J.-H. Chu, H.-H. Kuo, J. G. Analytis, and I. R. Fisher, Science **337**, 710 (2012).
[8] X. Lu, J. T. Park, R. Zhang, H. Luo, A. H. Nevidomskyy, Q. Si, and P. Dai, Science **345**, 657 (2014).
[9] S.-H. Baek, D. V. Efremov, J. M. Ok, J. S. Kim, J. van den Brink, and B. Büchner, Nat Mater (2014).
[10] A. E. Böhmer and C. Meingast, Comptes Rendus Physique , (2015).
[11] A. V. Chubukov, M. Khodas, and R. M. Fernandes, Phys. Rev. X **6**, 041045 (2016).
[12] Y. Gallais and I. Paul, Comptes Rendus Physique **17**, 113 (2016).
[13] A. P. Dioguardi, T. Kissikov, C. H. Lin, K. R. Shirer, M. M. Lawson, H.-J. Grafe, J.-H. Chu, I. R. Fisher, R. M. Fernandes, and N. J. Curro, Phys. Rev. Lett. **116**, 107202 (2016).
[14] Y. Schattner, S. Lederer, S. A. Kivelson, and E. Berg, Phys. Rev. X **6**, 031028 (2016).
[15] L. Classen, R.-Q. Xing, M. Khodas, and A. V. Chubukov, Phys. Rev. Lett. **118**, 037001 (2017), and refs therein.
[16] P. O. Sprau, A. Kostin, A. Kreisel, A. E. Böhmer, V. Taufour, P. C. Canfield, S. Mukherjee, P. J. Hirschfeld, B. M. Andersen, and J. C. S. Davis, Science **357**, 75 (2017).
[17] See Supplemental Material at [*url put by publisher*] for details of data analysis, phonon spectra and the spectra in the superconducting state.
[18] T. M. McQueen, A. J. Williams, P. W. Stephens, J. Tao, Y. Zhu, V. Ksenofontov, F. Casper, C. Felser, and R. J. Cava, Phys. Rev. Lett. **103**, 057002 (2009).
[19] A. E. Böhmer, T. Arai, F. Hardy, T. Hattori, T. Iye, T. Wolf, H. v. Löhneysen, K. Ishida, and C. Meingast, Phys. Rev. Lett. **114**, 027001 (2015).
[20] S. Hosoi, K. Matsuura, K. Ishida, H. Wang, Y. Mizukami, T. Watashige, S. Kasahara, Y. Matsuda, and T. Shibauchi, Proc. Natl. Acad. Sci. USA **113**, 8139 (2016).
[21] M. A. Tanatar, A. E. Böhmer, E. I. Timmons, M. Schütt, G. Drachuck, V. Taufour, K. Kothapalli, A. Kreyssig, S. L. Bud'ko, P. C. Canfield, R. M. Fernandes, and R. Prozorov, Phys. Rev. Lett. **117**, 127001 (2016).
[22] P. Massat, D. Farina, I. Paul, S. Karlsson, P. Strobel, P. Toulemonde, M.-A. Masson, M. Cazayous, A. Sacuto, S. Kasahara, T. Shibauchi, Y. Matsuda, and Y. Gallais, Proc. Natl. Acad. Sci. USA **113**, 9177 (2016).
[23] A. Baum, H. N. Ruiz, N. Lazarević, Y. Wang, T. Böhm, R. Hosseinian Ahangharnejhad, P. Adelmann, T. Wolf, Z. V. Popović, B. Moritz, T. P. Devereaux, and R. Hackl, ArXiv e-prints (2017), 1709.08998.
[24] M. D. Watson, T. K. Kim, L. C. Rhodes, M. Eschrig, M. Hoesch, A. A. Haghighirad, and A. I. Coldea, Phys. Rev. B **94**, 201107 (2016).
[25] A. I. Coldea and M. D. Watson, Annu. Rev. Condens. Matter Phys. **9**, 125 (2018).
[26] A. Fedorov, A. Yaresko, T. K. Kim, Y. Kushnirenko, E. Haubold, T. Wolf, M. Hoesch, A. Grüneis, B. Büchner, and S. V. Borisenko, Sci. Rep. **6**, 36834 (2016).
[27] H. C. Xu, X. H. Niu, D. F. Xu, J. Jiang, Q. Yao, Q. Y. Chen, Q. Song, M. Abdel-Hafiez, D. A. Chareev, A. N. Vasiliev, Q. S. Wang, H. L. Wo, J. Zhao, R. Peng, and D. L. Feng, Phys. Rev. Lett. **117**, 157003 (2016).
[28] W. Qing-Yan, L. Zhi, Z. Wen-Hao, Z. Zuo-Cheng, Z. Jin-Song, L. Wei, D. Hao, O. Yun-Bo, D. Peng, C. Kai, W. Jing, S. Can-Li, H. Ke, J. Jin-Feng, J. Shuai-Hua, W. Ya-Yu, W. Li-Li, C. Xi, M. Xu-Cun, and X. Qi-Kun, Chin. Phys. Lett. **29**, 037402 (2012).
[29] J.-F. Ge, Z.-L. Liu, C. Liu, C.-L. Gao, D. Qian, Q.-K. Xue, Y. Liu, and J.-F. Jia, Nat Mater **14**, 285 (2015).
[30] D.-H. Lee, Science **357**, 32 (2017).
[31] T. Hanaguri, K. Iwaya, Y. Kohsaka, T. Machida, T. Watashige, S. Kasahara, T. Shibauchi, and Y. Matsuda, ArXiv e-prints (2017), arXiv:1710.02276.
[32] K. Matsuura, Y. Mizukami, Y. Arai, Y. Sugimura, N. Maejima, A. Machida, T. Watanuki, T. Fukuda, T. Yajima, Z. Hiroi, K. Y. Yip, Y. C. Chan, Q. Niu, S. Hosoi, K. Ishida, K. Mukasa, T. Watashige, S. Kasahara, J.-G. Cheng, S. K. Goh, Y. Matsuda, Y. Uwatoko, and T. Shibauchi, (2017), arXiv:1704.02057.
[33] F. Kretzschmar, T. Bohm, U. Karahasanovic, B. Muschler, A. Baum, D. Jost, J. Schmalian, S. Caprara, M. Grilli, C. Di Castro, J. G. Analytis, J. H. Chu, I. R. Fisher, and R. Hackl, Nat. Phys. **12**, 560 (2016).
[34] V. Gnezdilov, Y. G. Pashkevich, P. Lemmens, D. Wulferding, T. Shevtsova, A. Gusev, D. Chareev, and A. Vasiliev, Phys. Rev. B **87**, 144508 (2013).
[35] Q. Wang, Y. Shen, B. Pan, Y. Hao, M. Ma, F. Zhou, P. Steffens, K. Schmalzl, T. R. Forrest, M. Abdel-Hafiez, X. Chen, D. A. Chareev, A. N. Vasiliev, P. Bourges, Y. Sidis, H. Cao, and J. Zhao, Nat. Mater **15**, 159 (2016).
[36] F. Kretzschmar, B. Muschler, T. Böhm, A. Baum, R. Hackl, H.-H. Wen, V. Tsurkan, J. Deisenhofer, and A. Loidl, Phys. Rev. Lett. **110**, 187002 (2013).
[37] A. Hinojosa, J. Cai, and A. V. Chubukov, Phys. Rev. B

93, 075106 (2016).
[38] V. K. Thorsmølle, M. Khodas, Z. P. Yin, C. Zhang, S. V. Carr, P. Dai, and G. Blumberg, Phys. Rev. B **93**, 054515 (2016).
[39] Y. Gallais, I. Paul, L. Chauvière, and J. Schmalian, Phys. Rev. Lett. **116**, 017001 (2016).
[40] S.-F. Wu, P. Richard, H. Ding, H.-H. Wen, G. Tan, M. Wang, C. Zhang, P. Dai, and G. Blumberg, Phys. Rev. B **95**, 085125 (2017).
[41] W.-L. Zhang, P. Richard, H. Ding, A. S. Sefat, J. Gillett, S. E. Sebastian, M. Khodas, and G. Blumberg, ArXiv e-prints (2014), arXiv:1410.6452.
[42] C.-C. Lee, W.-G. Yin, and W. Ku, Phys. Rev. Lett. **103**, 267001 (2009).
[43] W. Lv, J. Wu, and P. Phillips, Phys. Rev. B **80**, 224506 (2009).
[44] T. Saito, S. Onari, and H. Kontani, Phys. Rev. B **82**, 144510 (2010).
[45] H. Yamase and R. Zeyher, Phys. Rev. B **88**, 125120 (2013).
[46] H. Kontani and Y. Yamakawa, Phys. Rev. Lett. **113**, 047001 (2014).
[47] R.-Q. Xing, L. Classen, M. Khodas, and A. V. Chubukov, Phys. Rev. B **95**, 085108 (2017).
[48] W.-L. Zhang, Z. P. Yin, A. Ignatov, Z. Bukowski, J. Karpinski, A. S. Sefat, H. Ding, P. Richard, and G. Blumberg, Phys. Rev. B **93**, 205106 (2016).
[49] R. Yu and Q. Si, Phys. Rev. Lett. **115**, 116401 (2015).
[50] Q. Wang, Y. Shen, B. Pan, X. Zhang, K. Ikeuchi, K. Iida, A. D. Christianson, H. C. Walker, D. T. Adroja, M. Abdel-Hafiez, X. Chen, D. A. Chareev, A. N. Vasiliev, and J. Zhao, Nat. Commun. **7**, 12182 (2016).
[51] A. Kreisel, B. M. Andersen, P. O. Sprau, A. Kostin, J. C. S. Davis, and P. J. Hirschfeld, Phys. Rev. B **95**, 174504 (2017).
[52] P. Zhang, X.-L. Peng, T. Qian, P. Richard, X. Shi, J.-Z. Ma, B. B. Fu, Y.-L. Guo, Z. Q. Han, S. C. Wang, L. L. Wang, Q.-K. Xue, J. P. Hu, Y.-J. Sun, and H. Ding, Phys. Rev. B **94**, 104510 (2016).